Accurate quantitative EDS-TEM analysis of precipitates and matrix in equilibrium (α+β) Zr–1Nb alloys with Ta addition

P.A. Ferreirós, P.R. Alonso, D.P. Quirós, E. Zelaya, G.H. Rubiolo

PII: S0925-8388(20)32736-5

DOI: https://doi.org/10.1016/j.jallcom.2020.156372

Reference: JALCOM 156372

To appear in: *Journal of Alloys and Compounds*

Received Date: 11 May 2020

Revised Date: 9 July 2020

Accepted Date: 10 July 2020

Please cite this article as: P.A. Ferreirós, P.R. Alonso, D.P. Quirós, E. Zelaya, G.H. Rubiolo, Accurate quantitative EDS-TEM analysis of precipitates and matrix in equilibrium (α+β) Zr–1Nb alloys with Ta addition, *Journal of Alloys and Compounds* (2020), doi: https://doi.org/10.1016/j.jallcom.2020.156372.

Credit Author Statement

P.A. Ferreirós: Conceptualization, Methodology, Validation, Formal analysis, Investigation, Writing- Reviewing and Editing, Visualization. **P.R. Alonso**: Resources, Writing- Reviewing and Editing, Supervision. **D.P. Quirós**: Resources, Investigation. ***E. Zelaya****:* Investigation, Writing - Review & Editing.**: G.H. Rubiolo**: Conceptualization, Validation, Writing- Reviewing and Editing, Supervision, Project administration, Funding acquisition.

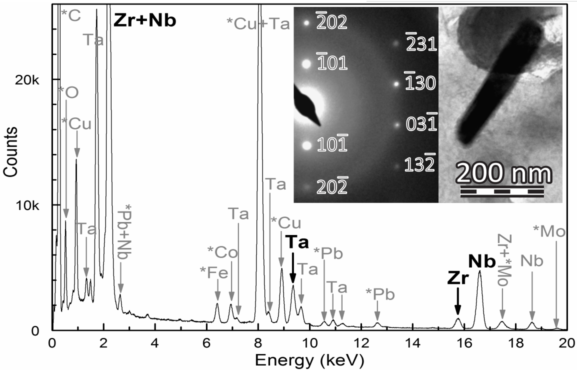
Zr+Nb
Counts
Energy (keV)
0
10k
20k
0
2
4
6
8
10
12
14
16
18
20
*C
Ta
*O
*Cu
Ta
*Pb+Nb
*Fe
*Co
Ta
*Cu+Ta
Ta
*Cu
Ta
Ta
*Pb
Ta
*Pb
Zr
Nb
Zr+*Mo
Nb
*Mo
2̄02
1̄01
101̄
202̄
2̄31
1̄30
031̄
132̄
200 nm

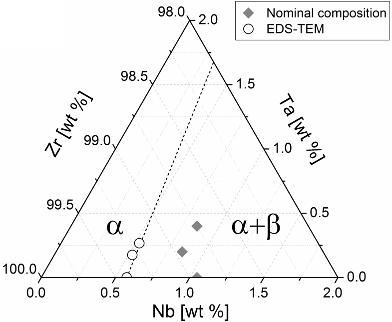
◆ Nominal composition
○ EDS-TEM
Zr [wt %]
Ta [wt %]
Nb [wt %]
98.0
98.5
99.0
99.5
100.0
2.0
1.5
1.0
0.5
0.0
0.0
0.5
1.0
1.5
2.0
α
α+β

Accurate quantitative EDS-TEM analysis of precipitates and matrix in equilibrium (α+β) Zr-1Nb alloys with Ta addition

P.A. Ferreirós[a,b,c,*], P.R. Alonso[a], D.P. Quirós[a], E. Zelaya[d], G.H. Rubiolo[a,c]

[a] Gerencia Materiales (GAEN) - Comisión Nacional de Energía Atómica (CNEA), Instituto Sabato - Universidad Nacional de San Martín (UNSAM), Av. Gral. Paz 1499, San Martín, Buenos Aires B1650KNA, Argentina.
[b] Facultad Regional Haedo (UTN-FRH), Universidad Tecnológica Nacional, París 532, Haedo, B1706EAH Buenos Aires, Argentina.
[c] Consejo Nacional de Investigaciones Científicas y Técnicas (CONICET), Godoy Cruz 2290, C1425FQB Ciudad Autónoma de Buenos Aires, Argentina.
[d] Centro Atómico Bariloche (CAB), CONICET, Avenida Bustillo 9500, San Carlos de Bariloche, Río Negro, R8402AGP, Argentina.

Abstract

The (α+β) phase microstructure in Zr-1.05Nb, Zr-0.85Nb-0.20Ta and Zr-0.85Nb-0.40Ta (wt.%) alloys annealed at 570 °C for 3840 h after β-quenching were observed at different scales by optical, SEM and TEM microscopies. A quantitative study of phase chemical compositions was carried out by EDS-TEM with experimental Cliff-Lorimer factors. The α matrix was measured on thin films and the β particle on carbon extractive replicas. The Ta addition showed a continuous increase of (Nb+Ta) solubility in α-Zr and (Zr+Ta) solubility in the β-Nb phase. The increase of Ta in the nominal composition of the Zr-1(Nb, Ta) alloy causes the decrease of the mass fraction of β-Nb phase.

Keywords: Zr-Nb alloys; Ta addition; Transmission electron microscopy (TEM); Energy dispersive X-ray spectroscopy (EDS); Cliff-Lorimer factor.

1. Introduction

Zirconium alloys have a low thermal neutron absorption cross-section, and this positioned them as base material in fuel channels and fuel assemblies of all conventional nuclear reactors that generate power from the fission of uranium by thermal neutrons [1,2]. There

---

[*] Corresponding author. Present address: Gerencia de Materiales, Departamento de Transformaciones y Propiedades, Comisión Nacional de Energía Atómica, Av. Gral. Paz 1499, B1650KNA San Martín, Argentina. Tel.: 054 11 6772 7247; Fax: 054 11 6772 7362.

E-mail address: ferreiros@cnea.gov.ar (P.A. Ferreirós)

is a wide variety of zirconium alloys, among which modern alloys such as Zr-1Nb and Zr-1Sn-1Nb (wt.%) stood out. The M5 (trademark of AREVA NP, France) and E110 (produced by TVEL, the Russian nuclear vender) alloys belong to the first group and Zirlo (trademark of Westinghouse Electric Company LLC, USA) alloy to the second group [3,4,5]. Since the development stage of these alloys, corrosion resistance is known to increase when equilibrium particles of β-Nb phase (very rich in Nb) are present instead of the metastable β-Zr phase (19 wt.% Nb) [6,7,8]. Although several authors claim that it is the Nb concentration in α matrix, rather than the presence of equilibrium particles, the dominant factor to control the corrosion kinetics. However, both approaches are not opposed because the β-Nb particles are formed by extracting Nb from the α matrix up to its solubility limit [9,10,11,12,13]. A very recent research provided new experimental information and with it builds a very convincing new hypothesis of the role that Nb plays during water corrosion [6]. The authors show that the amount of Nb ions distributed in solution in the oxide increases the parabolicity of the oxidation kinetics of Zr-Nb. Furthermore, they demonstrated that β-Zr precipitates dissolve during oxidation supplying Nb to the oxide surrounding matrix, while dissolution of β-Nb precipitates is much slower and makes these precipitates more effective in retaining Nb and retarding oxidation. The authors can explain their experimental results with the hypothesis that the space charge within the oxide can be compensated by aliovalent ions dispersed in solution; the lower the concentration of aliovalent ions in solution, the less the space charge compensation and a subparabolic oxidation kinetics occurs.

Recently the Zr-1.5Nb-1Ta (at.%) alloy was tested to evaluate its corrosion in vitro with the aim of using it as a biological implant material [14,15]. The passive oxide film formed on the alloy surface protects from subsequent corrosion more efficiently than the passive film formed on Ti Grade 2 and the well-known nuclear Zr-2.5Nb (wt%) alloy. Unlike Nb, the Ta addition in Zr-base alloys has no background in the literature regarding the corrosion under water at high pressure and temperature.

In Zr-base alloys for nuclear applications the Ta addition was also a slightly explored field so far [16,17,18]. The binary phase diagrams Zr-Nb and Zr-Ta have similar phase fields; both have a monotectoid reaction and a low solubility of Nb and Ta in the α-Zr phase [19,20,21,22]. On the other hand, the Nb-Ta diagram has a continuous solid solution bcc (β phase) [23,24,25]. Therefore, for small additions of Ta in Zr-1Nb type alloys and temperatures below the monotectoid, it is expected that the two-phase microstructure (α-Zr + β-Nb) remains and that Ta atoms also tend to form the β-Nb precipitate.

Consequently, this article focuses on the influence of a small addition of Ta on the phase equilibrium microstructure of the Zr-1% Nb alloy aged at 570 °C. By means of selected area electron diffraction (SAED) and quantitative energy dispersion spectroscopy (EDS) performed with a transmission electron microscope (TEM), the crystal structure and chemical composition of Nb-rich precipitates extracted in carbon replicas were characterized. Then, the EDS-TEM technique was applied to alloy thin films to measure the solubility of Nb and Ta in the matrix phase when Ta is added to the Zr-1% Nb alloy. Commonly, quantitative methods to measure Nb content in a Zr matrix have high uncertainty due to the similar atomic structure and the low solubility limit. The large spread in the reported values for Nb content in α-Zr matrix (0.07-0.6 at% [26,27,28]), makes the Nb solubility limit uncertain. It has even been difficult to achieve an accurate estimate using the high resolution of the Atom Probe Tomography technique [9,29,30], because the measurement volume is so small that the representativeness of the bulk sample is lost [31,32]. The addition of Ta as a third alloy element could bring more uncertainty in certain measurement techniques. This would be the case of chemical accurate quantitative measurements by the EDS-TEM technique using experimental Cliff-Lorimer factors [33]. Since Ta has a large atomic mass, the critical energy to ionize its K shell is not reached with the usual TEM voltages [34]. Therefore, the Cliff-Lorimer method must be performed with the L layer signals, but these signals coming from the Nb and Zr atoms overlap. However, these drawbacks can be addressed with a carefully analysis presented in depth and discussed as part of this paper.

2. Materials and methods

All the alloys used in this study were melted in an electric arc furnace with tungsten electrode and water cooled copper crucible under argon atmosphere. The samples were turned and remelted several times to ensure homogeneity. In the melting process, weight losses of less than 0.04 % were obtained. The used raw materials were sponge Zr (628 ± 63 ppm O, 148 ±24 ppm Fe, 68 ±16 ppm Hf and 30 ±4 ppm N) and pure elements, Nb and Ta, with purity better than 99.9 wt.%.

2.1 Standard alloys for the determination of X-ray intensity k ratios

Two alloy buttons of 18 g were melted with the nominal chemical compositions pointed out in Table 1. Then, using a low speed diamond saw, each button was cut into halves for further compositional evaluation. The homogeneity of the alloys was evaluated by measuring their average chemical compositions by means of electron probe micro-analysis (EPMA) in a Cameca SXFive equipment using three wavelength dispersive X-ray spectrometers (WDS). Pure element standards provided by CAMECA were used for calibration. Conventional ZAF matrix correction routine incorporated into the Cameca's PeakSight software was used to calculate the final compositions. The accuracy of one composition measurement in this scheme has a standard deviation of ±2% relative [35]. The values were obtained from the average and standard deviation of 200 measurements along a straight line of 8 mm with a 10 µm spot diameter (see Table 1). The uncertainty range of the measured average chemical composition considering the accuracy standard deviation in one EPMA measurement includes the value of the nominal chemical composition of standard alloys according to the fact of a very low weight loss during the melting.

Table 1. Chemical compositions of standard alloys.

Nominal composition (wt%)	EPMA composition (wt.%)		
	Zr	Nb	Ta
(St-1) 12.5Zr-46.5Nb-41Ta	12.45 ±0.10	46.43 ±0.25	41.12 ±0.27
(St-2) 66Zr-18Nb-16Ta	66.22 ±0.54	17.94 ±0.14	15.84 ±0.13

These two standard alloys were used to characterize the experimental sensitivity Cliff-Lorimer factors (k) of the EDS-TEM spectra obtained with a field emission TEM FEI Tecnai F20 G2 (FEG) operated at 200 kV with an EDAX EDS detector, take-off angle 14.8°, sample rotation 15° and data collected from a focused spot of 15 nm diameter. Thin films of the standard alloys with a homogeneous thickness below 100 nm were prepared in a SEM/FIB FEI Quanta 3d 200i. Through conventional focused ion beam (FIB) milling process, a lamella was lift out from the half button, then welded to a copper TEM holder and FIB-milled to the final thickness.

At least ten EDS spectra were measured in different parts of each thin-foil standard. From the statistical point of view, the level of homogeneity previously analyzed by EPMA ensures that the data taken for the X-ray counts at certain energy in each EDS scan can be handled as a sample taken from the same distribution. Because the X-ray counts (n) in the spectrum obey the Poisson statistic, its statistic fluctuation is $\sqrt{n}$. It follows for a relatively simple integration that the number of counts in a peak above the background has a statistic fluctuation equal to the square root of those counts. Therefore, if the X-ray counts from N individual spectra are summed, the intensity background corrected of the peak increases N times while the statistical fluctuation increases as $\sqrt{N}$ times, so the relative error in the peak intensity will decrease as $\left(1/\sqrt{N}\right)$ times. Since the Cliff-Lorimer method uses intensity background corrected ratio, their accuracy will be greatly improved if we use the summed spectra. Prior to obtain the sum spectrum, those individual spectra that do not fulfilled the statistical similarity requirements are discarded. The procedure was as follows. First, using the DTSA-II software [36], the individual spectra were normalized setting the intensity of a representative peak to be the same in all of them. Then, all normalized individual spectra were compared in pairs to verify similarity using the statistical method reported in the reference [37].

The sum EDS-TEM spectra of each thin film standards used to characterize the k factors are shown in Fig. 1. The quantified lines are highlighted in black and lines from chemical element coming from materials external to the sample are marked with an asterisk (internal parts of the TEM and Cu holder). The methodology to determine the k_{ZrNb}, k_{ZrTa} and k_{NbTa} factors from the data in Fig. 1 and the Cliff-Lorimer equation [33] is detailed in the appendix. Table 2 shows the k values. No additional absorption and fluorescence corrections were made for this experimental scheme of k factors determination.

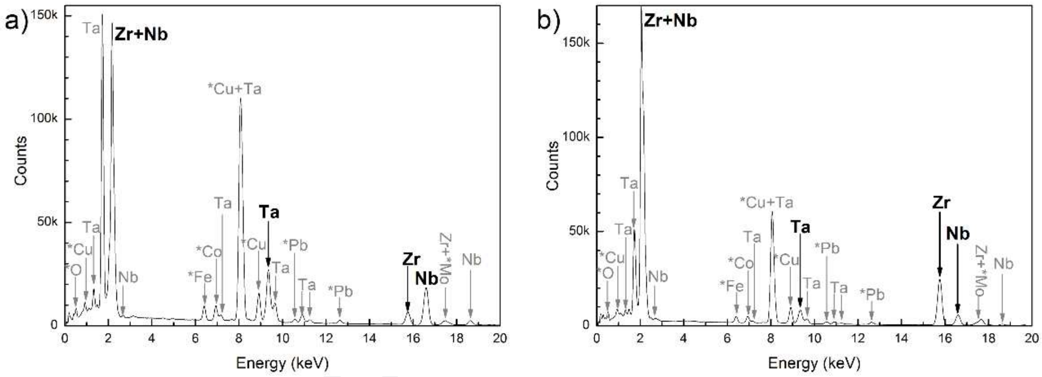

Fig. 1. Sum of EDS-TEM spectrum measured in a) St-1 (12.5Zr-46.5Nb-41Ta) and b) St-2 (66Zr-18Nb-16Ta).

Table 2. Experimental Cliff-Lorimer sensitivity factors from the standard alloys.

Elements (A-B)	Lines (element A)	Lines (element B)	k	Relative Error (%)
Zr-Nb	K-L2 + K-L3	K-L2 + K-L3	0.844	2.3
Zr-Ta	L3-M4 + L3-M5 + L2-M4	L2-M4	0.272	4.8
Nb-Ta	L3-M4 + L3-M5 + L2-M4	L2-M4	0.354	3.9

2.2 Zr-1%Nb alloys with Ta addition

Three alloy buttons of 25 g were melted with the nominal compositions shown in Table 3. The absolute error in the chemical composition was estimated considering the total weight loss in the melt successively assigned to each element of the alloy. The three alloys were wrapped in a Tantalum foil, encapsulated into a quartz tube which was evacuated and back-filled with argon, heat treated at 1100 °C for 30 minutes and followed by a water quenching (β quenched). Based on the results reported in reference [7], the thermodynamic equilibrium microstructure in the alloys was obtained with an annealing at 570 °C for 3840 h under Ar atmosphere in a sealed quartz tube.

Table 3. Chemical compositions of the Zr-1%Nb alloys with Ta addition.

Alloy	Nominal composition ± absolute error (wt.%)		
	Zr	Nb	Ta
Zr-1.05Nb	98.9485 ± 0.0004	1.052 ± 0.039	-
Zr-0.85Nb-0.20Ta	98.9483 ± 0.0003	0.851 ± 0.032	0.201 ± 0.032
Zr-0.85Nb-0.40Ta	98.7510 ± 0.0004	0.850 ± 0.035	0.399 ± 0.035

The metallographic surfaces for optical microscopy and scanning electron microscopy (SEM) were polished up to 600 grade abrasive paper and etched with 45% glycerin, 45% H_2SO_4 and 10% HF by swabbing for 25 s. The microscopes used were an Olympus BX60M and a FEI Quanta 200 respectively. The characterization of the precipitate phase was carried out in carbon extraction replicas [38]. The etched surface was covered by a carbon layer with a Quorum Q150T ES equipment. The detachment of the replica was carried out by chemical dissolution of the matrix phase with electro-etching (250 mA, 66 % methanol, 22 % 2-Butoxyethanol and 12 % perchloric acid). The crystalline structure and the qualitative chemical composition of the particles in the extractive replicas were analyzed by EDS-TEM using a Philips CM200 microscope operated at 160 kV and an EDAX detector. Thin films were prepared to study the matrix phase of the alloys. Discs of 3 mm diameter were cut and mechanically ground to a final thickness of 100 μm using SiC paper and thinned to electron transparency by electro-polishing (90% methanol, 10% perchloric acid at -30°C) using a Tenupol-5 Struers dual jet polisher. The chemical quantitative analyzes of precipitates (carbon extractive replicas) and matrix phase (thin films) were performed with the same EDS-TEM equipment and analysis conditions used for the determination of the k sensitivity factors explained in section 2.1. Also in these measurements the methodology was to collect at least ten EDS spectra in each phase and quantify their chemical composition with the sum spectrum.

3. Results

Optical micrographs of the alloys with thermal treatments of β quenching and subsequent equilibrium annealing are showed in Fig. 2. In the bright field micrographs, to the left of each image, it can be seen that the needles of the tempered martensitic phase were revealed. This is possible due to a preferential precipitation at the needle boundaries, as could be noticed from the bright field–dark field combination in the image of the same zone. The SEM examination of this microstructure shows a finer arrangement of smaller precipitates within the needles (Fig. 3). The formation of these precipitates is in narrow bands and these bands appeared to align along some specific crystallographic direction. The formation of aligned precipitates was also collected in the extractive replicas as shown in the TEM micrograph of Fig. 4a. In order to identify the precipitate phase, selected area electron diffraction (SAED) from the particles in the replica were taken (Fig. 4b) and their bright and dark field images are shown (Fig. 4c and 4d, respectively). Electron diffraction analysis confirmed that the precipitates were of the β phase (bcc). The qualitative EDS analysis of the particle indicated a high content of niobium and tantalum (Nb+Ta> 80 wt.%) and a low content of zirconium. Approximately 15 particles of each alloy's extraction replica were analyzed in the same way as reported for the particle in Fig 4. In all cases, the result was a low content of Zr (< 20 wt.%) and a bcc structure. Besides this β type precipitate, a much smaller amount of second phase particles was found in all three alloys, whose crystal structures could not be identified as a bcc structure. In these cases, the qualitative EDS analysis was performed on four particles extracted from each alloy, the binary Zr-1Nb and the ternary Zr-0.85Nb-0.20Ta. The compositional analysis (average values in wt.%) gives (41.60 ± 0.96)Zr, (41.80 ± 0.96)Nb, (13.0 ± 0.7)Fe and (3.60 ± 0.24)Cr in the intermetallic of the Zr-1Nb binary alloy, while the figures are (31.2 ± 0.7)Zr, (25.8 ± 1.9)Nb, (32.4 ± 1.8)Ta, (8.9 ± 0.5)Fe and (1.83 ± 0.13)Cr in the intermetallic of the Zr-0.85Nb-0.20Ta ternary alloy. In this work, neither the crystalline structure nor the quantitative composition of these second phase particles is analyzed.

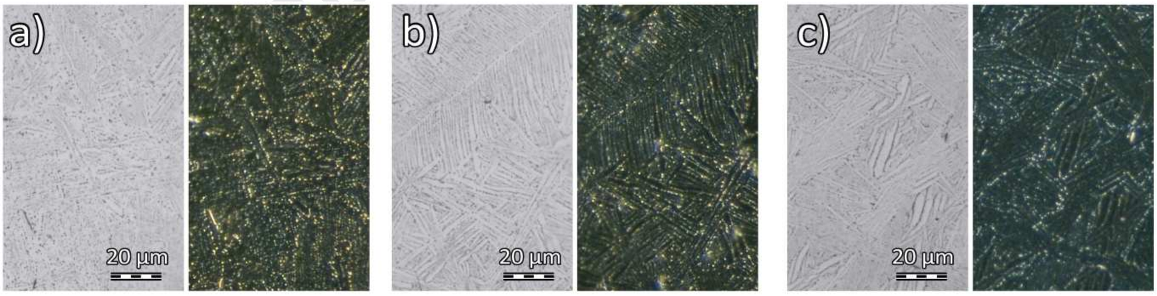

Fig. 2. Optical micrographs of alloys: a) Zr-1.05Nb, b) Zr-0.85Nb-0.20Ta and c) Zr-0.85Nb-0.40Ta. The precipitates are highlighted in the dark field micrographs as shown to the right of each image.

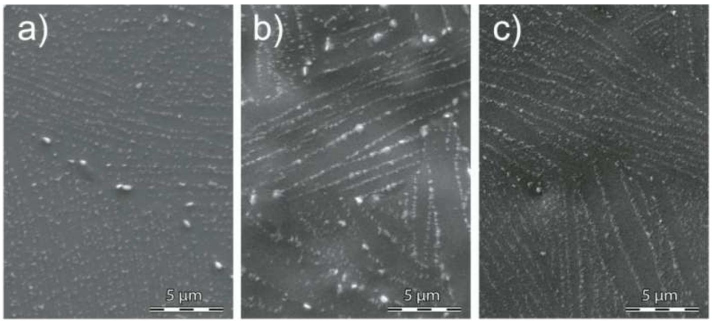

Fig. 3. SEM micrographs of alloys: a) Zr-1.05Nb, b) Zr-0.85Nb-0.20Ta and c) Zr-0.85Nb-0.40Ta.

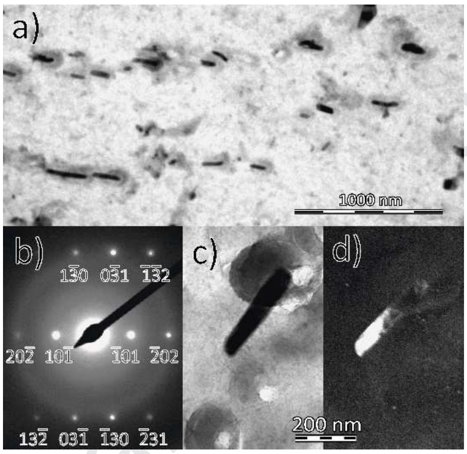

Fig. 4. TEM micrographs on carbon extractive replica of the Zr-0.85Nb-0.40Ta alloy. a) Bright field of a typical area of the replica, b) SAED pattern of a β particle, (313) zone axis, c) Bright field and d) $[10\bar{1}]$ dark field of the same particle.

In Zr-xNb (0.55 ≤ x %wt. ≤ 2.5) alloys, C. Toffolon et al. showed that up to 2000 hours of isothermal treatments at 570 °C were necessary for the β-Nb particles to be close to thermodynamic equilibrium [7]. Even though the annealing time of the alloys in this study is greater than 2000 hs, we evaluated whether the thermodynamic equilibrium was reached after prolonged annealing by comparing the diffusion length with the width of the precipitate bands observed by SEM. Using the annealing conditions ($T = 570\,°C$, $t = 3840\,h$), the diffusional pre-exponential factor (D_0) and the diffusion activation energy (Q) of the alloying elements: $D_0^{Nb} = 6.6x10^{-6}\,m^2/s$, $D_0^{Ta} = 100\,m^2/s$, $Q^{Nb} = 131.9\,kJ/mol$, $Q^{Ta} = 293.1\,kJ/mol$ [39] a diffusion length of $0.46\,\mu m$ and $0.31\,\mu m$ is obtained for Nb and Ta, respectively. The Fig. 3 shows that the width of precipitates bands observed by SEM is about twice the calculated diffusion lengths as expected if the equilibrium condition were reached. Taking into account that metallographic observations by 2D microscopy tend to show larger band separations than the effective ones due to the low probability that the metallographic cut will be perpendicular to the needle boundaries, we can conclude that this result supports the hypothesis that the thermodynamic equilibrium was reached.

Assuming that the chemical equilibrium of phases was achieved, the chemical composition on different precipitates and points in the matrix should be similar. Then, we can use the same statistical argument outlined in section 2.1 to use the sum EDS-TEM spectrum instead of the average of the individual EDS-TEM spectra in the quantification of the chemical composition of precipitates and matrix phase. The sum of ten EDS-TEM spectra measured in the β phase precipitates (carbon replica) of the Zr-0.85Nb-0.40Ta alloy is shown in Fig. 5. The X-ray lines necessary for the chemical quantitative analisys are highlighted in black, the X-ray lines marked with an asterisk are associated with scattering contibutions of the microscope and the specimen holder (Cu grid). The method to compute the intensity background corrected of these lines is explained in the appendix for the case of the Zr-Ta-Nb standard alloys (see Fig. A.1). Table 4 shows the line intensities of α and β phases in the three alloys.

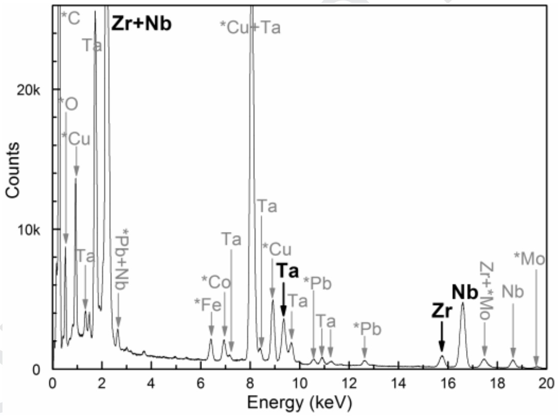

Fig. 5. Sum of EDS-TEM spectrum (N=10) measured in the carbon extractive replica of Zr-0.85Nb-0.40Ta alloy.

Table 4. Line intensities background corrected from the sum EDS-TEM spectra of the Zr-1%Nb alloys with Ta addition.

Alloy	Sample type	Phase	Element	Lines	keV	Intensity (counts x10^4)	Relative Error (%)
Zr-1.05Nb	Thin film	α	Zr	K-L2 + K-L3	15.8	226.82	0.20
			Nb	K-L2 + K-L3	16.6	1.11	2.85
Zr-0.85Nb-0.2Ta	Thin film	α	Zr+Nb	L3-M4 + L3-M5 + L2-M4	2.1	1193.41	0.09
			Ta	L2-M4	9.3	0.57	3.97
			Zr	K-L2 + K-L3	15.8	342.38	0.16
			Nb	K-L2 + K-L3	16.6	1.52	2.43
Zr-0.85Nb-0.4Ta	Thin film	α	Zr+Nb	L3-M4 + L3-M5 + L2-M4	2.1	1152.94	0.09
			Ta	L2-M4	9.3	0.84	3.27

			Zr	K-L2 + K-L3	15.8	371.96	0.16
			Nb	K-L2 + K-L3	16.6	1.66	2.33
Zr-1.05Nb	Replica	β	Zr	K-L2 + K-L3	15.8	3.90	1.52
			Nb	K-L2 + K-L3	16.6	15.89	0.75
Zr-0.85Nb-0.2Ta	Replica	β	Zr+Nb	L3-M4 + L3-M5 + L2-M4	2.1	188.67	0.22
			Ta	L2-M4	9.3	8.82	1.01
			Zr	K-L2 + K-L3	15.8	13.72	0.81
			Nb	K-L2 + K-L3	16.6	61.09	0.38
Zr-0.85Nb-0.4Ta	Replica	β	Zr+Nb	L3-M4 + L3-M5 + L2-M4	2.1	137.53	0.26
			Ta	L2-M4	9.3	10.84	0.91
			Zr	K-L2 + K-L3	15.8	3.77	1.54
			Nb	K-L2 + K-L3	16.6	22.91	0.63

4. Discussion

As it was showed previously by other authors [40], in binary Zr-Nb alloys containing more than 0.8 wt.% Nb, the β quenching produced an acicular martensite with internal twinning on $\{10\bar{1}1\}$ planes. Annealing of this martensitic structure at temperatures between 500 and 600 °C results in a clearly resolvable precipitation along the twin boundaries, while precipitation in the matrix was observed only occasionally [41]. At short annealing times the precipitates are identified as the metastable β-Zr phase, further annealing time promotes the diffusion of Nb and the equilibrium condition of β-Nb precipitates and α matrix could be reached [42]. In addition to the precipitation of the second phase, it was discovered that the internal twins shrink or disappear completely, leaving a discontinuous series of precipitates along the pre-existing twin boundaries. Our observations made with optical (Fig. 2) and electron (Fig. 3 and 4) microscopies agree with the characteristics of the precipitation mechanism outlined above and therefore allow us to conclude that the addition of a small amount of Ta to the alloys of Zr-1% Nb does not affect it.

In addition to these findings, our results in Table 4 can accurately assess the composition and mass fraction of both phases, matrix and major precipitates, in thermodynamic equilibrium. First, these results together with the Cliff-Lorimer sensitivity factors in Table 2 and the system of Eq. (A.1), (A.2) and (A.3) allow us to calculate the chemical composition of the phases. Then, neglecting other minor phases, the mass fraction of both α matrix and β-Nb phases are calculated.

The chemical compositions obtained for each phase in the three alloys are displayed in Fig. 6. The error bars in these plots represent the total error as obtained from the propagation of relative errors of intensities lines and sensitivity factors in the mathematical expressions for chemical concentrations that are solution to the system of Eq. (A.1), (A.2) and (A.3). Because the atomic mass of Ta is approximately twice that of Zr or Nb, Fig. 7 shows the same results as in Fig. 6 for the chemical compositions now calculated as atomic fraction (at.%).

For the binary alloy, our measured value of 0.574 ± 0.077 wt.% Nb for the terminal solid solubility of Nb in the α phase at 570 °C is within the range of experimental values compiled by Abriata and Bolcich [28] ranging between 0.5 to 6.4 wt.% and close to the maximum value of the range 0.29-0.49 wt.% suggested in the review report of Harte et al. [43]. In the ternary alloys containing Ta, it appears that Ta slightly reduces the solubility of Nb in the α phase while increasing the total solubility (see Fig. 7).

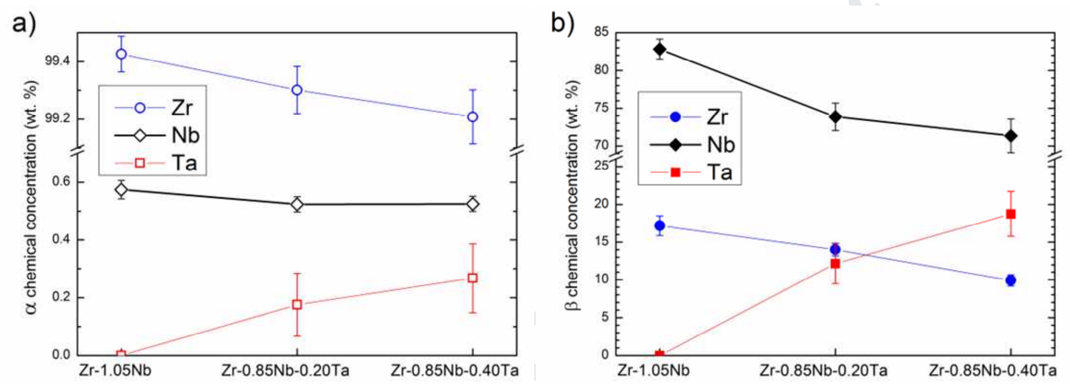

Fig. 6. Mass fraction chemical concentrations of (a) α phase and (b) β phase.

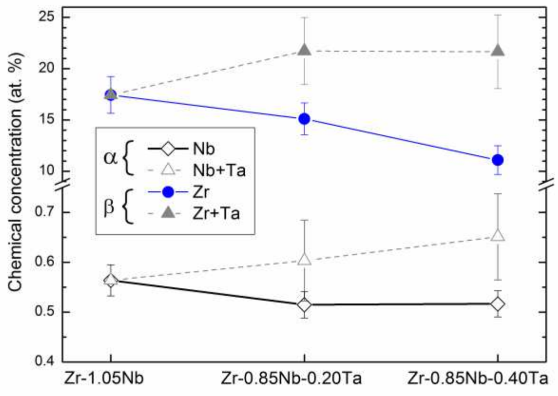

Fig. 7. Atomic fraction chemical concentration of Nb or (Nb+Ta) in the α phase and Zr or (Zr+Ta) in the β phase.

The composition range for the β-Nb phase in binary Zr-Nb alloys is analyzed by Harte taking sixty studies from the literature [43], predominantly with demonstrated zero concentration of Fe; the measured values show a distribution whose average is 87.7 wt.% Nb and its standard deviation is 4.6 wt.%. Our measured value of 82.8 ± 1.3 wt.% Nb for the β-Nb phase at 570 °C overlaps with the lower part of that range. As expected, Ta is a stronger β-stabilizer than Zr, it reduces the solubility of Zr but increases the total solubility in the β phase (see Fig. 7).

Woo and Griffiths [44] have well-characterized the appearance of various phases in "binary" Zr-Nb systems with impurities of Fe, and, to a lesser extent, Cr, Ni, Cu and W; they found that for contents higher than 0.2 wt.% Nb and 24 ppm Fe alloys predominantly nucleate ZrNbFe intermetallics and the β-Nb phase. The extensive study of model ternary Zr-Nb-Fe alloys by Argentinian groups [45,46] and French groups [47,48] have reported the existence of two dominant ternary ZrNbFe phases: the hexagonal $Zr(Nb,Fe)_2$ and the face-centered cubic $(Zr,Nb)_2Fe$. The Zr content of our results in the intermetallic particles, expressed in at.%, is (37.7 ± 0.98) for the binary alloy and (34.45 ± 0.9) for the ternary alloy; these values fit well with the stoichiometric assignment $Zr(Nb,Fe)_2$ considering the average value (35.6 ± 5.0) at.% obtained from 112 measurements compiled by Harte et al. [43] from those reported in the literature.

Fig. 8a shows the mass fraction of both α matrix and β-Nb phases, even when the observed changes are small, it is noted that the addition of Ta causes a decrease in the mass fraction of the beta phase. The effect is strong at low addition and then remains almost constant. The reason for this behavior is understandable by analyzing Fig. 8b, the alpha phase boundary measured in this study falls on a line that is parallel to the line supported by the nominal compositions of alloys Zr-0.85Nb-0.20Ta and Zr-0.85Nb-0.40Ta while the nominal composition of the Zr-1Nb alloy is furthest from that phase boundary. As a corollary, we note that the measured alpha phase boundary is consistent with a much larger limit of Ta solubility in the α-Zr phase [20,21,22].

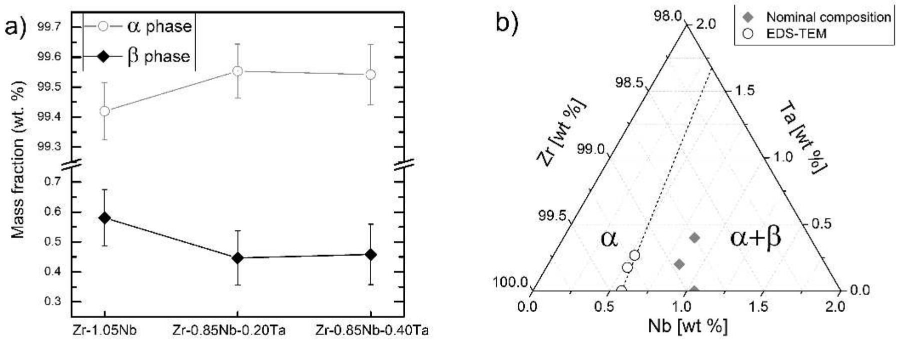

Fig. 8. a) Phase mass fraction in the studied Zr-Nb-Ta alloys; b) The zirconium apex of the ternary system Zr-Nb-Ta showing the results of this work.

The results of our research indicate that Ta addition in Zr-1Nb alloy maintains the two-phase microstructure of Zr-1Nb nuclear alloys and could be considered as a potential alloying element to modify the corrosion kinetics under water at high pressure and temperature. In this regard, following the corrosion kinetics model in Ref. [6], the two important effects to pay particular attention are the behavior as aliovalent ion in solution within zirconia (i.e, its average oxidation state) and in its power to prevent the dissolution of the β-zirconium or β-niobium phase particle. A forthcoming publication will show our findings in this regard.

5. Conclusion

The (α+β) phase microstructure in Zr-1.05Nb, Zr-0.85Nb-0.20Ta and Zr-0.85Nb-0.40Ta (wt.%) alloys quenched from β phase and post equilibrium treatment (570 °C for 3840 h) were studied at different scales by optical, scanning electron and transmission electron microscopies. The martensitic needles of α phase (matrix) are decorated on boundaries by β phase particles and also inside with the particles aligned in parallel lines.

The chemical compositions of the phases were quantitatively measured by the EDS-TEM technique using standard X-ray intensity ratios for the Cliff-Lorimer method. Matrixes were measured on thin films and particles on carbon extractive replicas. The Ta addition showed a continuous increase of solubility of (Nb+Ta) in α-Zr and (Zr+Ta) in the β-phase. However, in both cases, the Ta atoms replace the majority solute atom. Holding the composition of (Nb+Ta) close to 1 wt.% in the nominal composition of the ternary Zr-Nb-Ta alloy causes the decrease in the mass fraction of the β-phase.

Acknowledgments

This study was supported by FONCYT, through PICT-2015-2267 project. The authors would like to thank MSc Diego Pérez from Departamento de Micro y Nanotecnología - Gerencia Desarrollo Tecnológico y Proyectos Especiales (GAIANN) for the FIB samples preparation.

Appendix

This section details the experimental determination, using standards alloys, of the sensitivity k factors required to quantify the chemical compositions of phases occurring in Zr-Nb-Ta alloys from the EDS spectra. Given that k factors are dependent on the equipment and measurement conditions, in this work all quantitative EDS analysis were performed with the same conditions.

In section 2.1 of this paper, we have detailed how standard alloys were manufactured and how their homogeneity and average chemical composition were evaluated using EPMA. It was also discussed there why the accuracy of the sensitivity k factors will be greatly improved if we use the summed spectra of ten individual EDS-TEM spectra taken on different parts of the thin sheet of the standard alloy. The sum EDS-TEM spectra of each thin film standards was shown in Fig. 1 detailed amplification of the spectrum around the quantized lines, highlighted in black in Fig. 1, are shown in Fig. A.1.

The experimental determination of the sensitivity k factors is relatively easy, in principle, you have to place a thin specimen of known composition, for example C_A and C_B, in the microscope, generate a spectrum, obtain values of I_A and I_B and insert those values in the Cliff-Lorimer equation [33]:

$$\frac{C_A}{C_B} = k_{AB}\,\frac{I_A}{I_B}$$

However, there is one thing that is often not highlighted, the relation between line intensities must be made with X-ray signals from the same electron shell (eg, K, L, M, etc.). In this regard, Zr-Nb-Ta ternary alloys have two drawbacks that must be overcome. First, tantalum is a heavy element and the critical ionization energy of the innermost shell (K) is too high to be reached by the voltage used in TEM. Therefore, in these alloys it is necessary to use the family of L lines instead of K lines. Then, a second problem arises, the L lines of the Zr and Nb are very close and their peaks are overlapping (Figs. A.1a and A.1d). This overlaping is not easy to resolvable by peaks deconvolution without introduce artifacts into intensities determination that we prefer to avoid. To try to solve all the mentioned drawbacks, we present an alternative method that uses two standard alloys instead of one and no peak deconvolution.

The method consists of the following. In the EDS-TEM spectrum of each standard alloy we will measure the individual intensities of the K lines of Zr and Nb, I_{Zr}^{K} and I_{Nb}^{K}, the sum of their intensities of lines L, $(I_{Zr}^{L} + I_{Nb}^{L})$, and the intensity of line L of Ta, I_{Ta}^{L}. Considering the Cliff-Lorimer equation we can write,

$$\frac{C_{Zr}}{C_{Nb}} = k_{ZrNb}^{K}\,\frac{I_{Zr}^{K}}{I_{Nb}^{K}} \qquad (A.1)$$

$$(I_{Zr}^{L} + I_{Nb}^{L}) = \frac{I_{Ta}^{L}}{C_{Ta}}\left(\frac{C_{Zr}}{k_{ZrTa}^{L}} + \frac{C_{Nb}}{k_{NbTa}^{L}}\right) \qquad (A.2)$$

Eq. A.1 is redundant to use on two different alloys to determine k_{ZrNb}^{K} beyond providing an estimate of its measurement error. On the contrary, Eq. A.2 used on two alloys of different chemical composition provides a system of equations to estimate the intensity factors k^L_{ZrTa} and k^L_{NbTa}. An additional problem arises using the copper holder of the thin sheet, the most intense L line of Ta ($Ta_{L3\text{-}M5}$) overlaps the $Cu_{L2\text{-}M3}$ line. But this was easily solved using the $Ta_{L2\text{-}M4}$ line. Because the $Ta_{L2\text{-}M4}$ line is slightly overlapped with the $Ta_{L3\text{-}N4+5}$ line, a Gaussian function was used to fit the peak shape and calculate the integral intensity (see Figs. A.1b and A.1e). The intensities of lines were calculated by subtracting the background contribution with a straight line beneath of each peak. The intensity (counts) is obtained as the mathematical peak integral divided the energy resolution (5 eV per channel). The intensity relative error (E), with a 99.7 % confidence limit, was calculated as: $E = \frac{3\, I^{\frac{1}{2}}}{I}$.

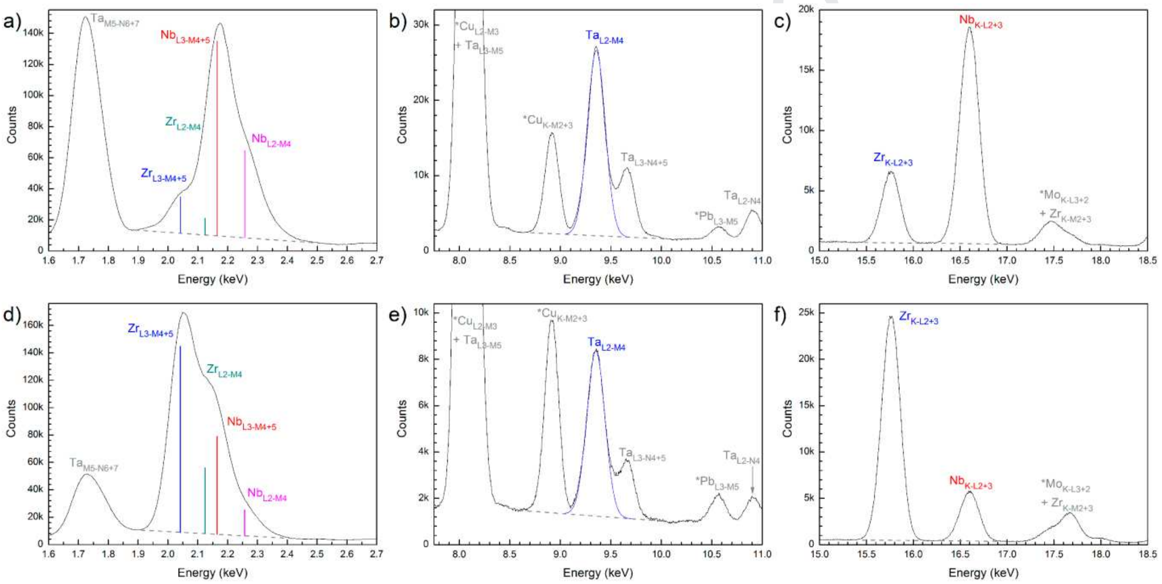

Fig. A.1. Detail of the EDS line intensities to quantify from the Fig. 1 spectra. St-1 (12.5Zr-46.5Nb-41Ta) in a), b) and d), St-2 (66Zr-18Nb-16Ta) in d), e) and f).

Table A.1. Intensity lines from sum of EDS spectra.

Alloy	Element	Lines	keV	Intensity (counts x10^5)	Relative Error (%)
(St-1) 12.5Zr-46.5Nb-41Ta	Zr+Nb	L3-M4 + L3-M5 + L2-M4	2.1	46.60	0.14
	Ta	L2-M4	9.3	10.84	0.29
	Zr	K-L2+3	15.8	2.86	0.56
	Nb	K-L2+3	16.6	9.09	0.31
(St-2) 66Zr-18Nb-16Ta	Zr+Nb	L3-M4 + L3-M5 + L2-M4	2.1	59.49	0.12
	Ta	L2-M4	9.3	3.21	0.53
	Zr	K-L2+3	15.8	11.83	0.28

	Nb	K-L2+3	16.6	2.68	0.58

The relative errors of sensitivity k factors in Table 2 of the main text are obtained from the propagation of relative errors in the mathematical expressions that are the solution of Eq. A.1 and the system of Eq. A.2. These mathematical expressions are functions of relative errors of line intensities (Table A.1) and chemical compositions (Table 1) measured in the standard alloys. The difference between the two values obtained for the sensitivity factor k_{ZrNb}^{K} using each standard alloy was less than the largest relative propagation error obtained from them.

Once the sensitivity k factors were determined, the measurement of the chemical composition in precipitates and matrices is obtained from the intensities I_{Zr}^{K} , I_{Nb}^{K} , $(I_{Zr}^{L} + I_{Nb}^{L})$ and I_{Ta}^{L2-M4} obtained in their EDS-TEM spectra and Eq. A.1 and A.2 together with the equation

$$C_{Zr} + C_{Nb} + C_{Ta} = 100 \qquad (A.3)$$

References

---

[1] R.B. Adamson, C.E. Coleman, M. Griffiths, Irradiation creep and growth of zirconium alloys: A critical review, J. Nucl. Mater. 521 (2019) 167-244

[2] Z. Duan, H. Yang, Y. Satoh, K. Murakami, S. Kano, Z. Zhao, J. Shen, H. Abe, Current status of materials development of nuclear fuel cladding tubes for light water reactors, Nucl. Eng. Des. 316 (2017) 131-150

[3] A.T. Motta, A. Couet, R.J. Comstock, Corrosion of Zirconium Alloys, Used for Nuclear Fuel Cladding, Annu. Rev. Mater. Res. 45 (2015) 311-43

[4] L. Hallstadius, S. Johnson, E. Lahoda, Cladding for high performance fuel, Prog. Nucl. Energ. 57 (2012) 71-76

[5] Y. Yan, T.A. Burtseva, M.C. Billone, High-temperature steam-oxidation behavior of Zr-1Nb cladding alloy E110, J. Nucl. Mater. 393 (2009) 433-448

[6] M. Moorehead, Z. Yu, L. Borrel, J. Hu, Z.Cai, A. Couet, Comprehensive investigation of the role of Nb on the oxidation kinetics of Zr-Nb alloys, Corros. Sci. 155 (2019) 173-181

[7] C. Toffolon, J.C. Brachet, T. Guilbert, D. Hamon, S. Urvoy, C. Servant, D. Charquet, L. Legras, J.P. Mardon, Vieillissement thermique des alliages de zirconium-niobium en phase α (570 °C), J. Phys. IVFrance 11 (2001) 99-108

[8] G. Yuan, L. Zhang, Q. Yue, H. Gu, G. Li, J. Shen, Microstructural characteristics of β precipitates in Zr-1Nb alloy, Mater. Chem. Phys. 165 (2015) 87-90

[9] Z. Yu, A. Couet, M. Bachhav, Irradiation-induced Nb redistribution of ZrNb alloy: An APT study, J. Nucl. Mater. 516 (2019) 100-110

[10] H.G. Kim, S.Y. Park, M.H. Lee, Y.H. Jeong, S.D. Kim, Corrosion and microstructural characteristics of Zr–Nb alloys with different Nb contents, J. Nucl. Mater. 373 (2008) 429-432

[11] Y.H. Jeong, H.G. Kim, T.H. Kim, Effect of β phase, precipitate and Nb-concentration in matrix on corrosion and oxide characteristics of Zr–xNb alloys, J. Nucl. Mater. 317 (2003) 1-12

[12] K.N. Choo, Y.H. Kang, S.I. Pyun, V.F. Urbanic, Effect of composition and heat treatment on the microstructure and corrosion behavior of Zr-Nb alloys, J. Nucl. Mater. 209 (1994) 226-235

---

[13] H.H. Klepfer, Zirconium — niobium binary alloys for boiling water reactor service part I — corrosion resistance, J. Nucl. Mater. 9 (1963) 65-76

[14] F. Rosalbino, D. Maccio, P. Giannoni, R. Quarto, A. Saccone, Study of the in vitro corrosion behavior and biocompatibility of Zr-2.5Nb and Zr-1.5Nb-1Ta (at%) crystalline alloys, J. Mater. Sci.: Mater Med. 22 (2011) 1293-1302

[15] F. Rosalbino, D. Maccio, G. Scavino, A. Saccone, Corrosion behavior of new ternary zirconium alloys as alternative materials for biomedical applications. Maters. Corros. 66 (2015) 1125-1132

[16] V.S. Emelianov, Iu.G. Godin, A.I. Evstiukhin, Study of the zirconium apex of the Zr-Ta-Nb phase diagram, The Soviet Journal of Atomic Energy 4 (1958) 211-220

[17] B. Cekić, K. Ćirić, M. Iordoc, S. Marković, M. Mitrić, D. Stojić, Kinetics of hydrogen absorption in Zr-based alloys, J. Alloy. Compd. 559 (2013) 162-166

[18] H. Sahan, E. Tel, M. Sahan, A. Aydin, I.H. Sarpun, A. Kara, M. Doner, A study on nuclear properties of Zr, Nb, and Ta nuclei used as structural material in fusion reactor, EPJ Web of Conferences 100,01007 (2015), DOI: 10.1051/epjconf/201510001007

[19] A. Fernández Guillermet, Phase diagram and thermochemical properties of the Zr-Ta system, An assessment based on Gibbs energy modelling, J. Alloy. Compd. 226 (1995) 174-184

[20] H. Okamoto, Ta-Zr (tantalum-zirconium), J. Phase Equilib. 17 (1996) 555

[21] H. Okamoto, Nb-Zr (Niobium-Zirconium), J. Phase Equilib. 13 (1992) 577

[22] R. Krishnan, S.P. Garg, S. Banerjee, N. Krishnamurthy, in T.B. Massalski, H.Okamoto, P.R. Subramanian and L. Kacprzak (eds.), Binary Alloy Phase Diag., ASM, Metals Park, OH, 2nd edn., 1990

[23] C. Ravi, B. K. Panigrahi, M. C. Valsakumar, and A. Van de Walle, First principles calculation of phase diagrams of V-Nb, V-Ta and Nb-Ta alloys, AIP Conference Proceedings 1447 (2012) 839-840

[24] K.C. Hari Kumar, T. Van Rompaey, P. Wollants, Thermodynamic calculation of the phase diagram of the Co–Nb–Ta system, Z. Metallkd. 93 (2002) 1146-1153

[25] Y. Liu, G. Wang, J. Wang, Z. Kang, Mobilities and diffusivities for bcc Nb–W, Nb–Ta, Zr–Mo and Zr–Hf alloys, J. Alloy. Compd. 555 (2013) 381-389

[26] Z. Yu, C. Zhang, P.M. Voyles, L. He, X. Liu, K. Nygren, A. Couet, Microstructure and microchemistry study of irradiation-induced precipitates in proton irradiated ZrNb alloys, Acta Mater. 178 (2019) 228-240

[27] M. Cottura, E. Clouet, Solubility in Zr-Nb alloys from first-principles, Acta Mater. 144 (2018) 21-30

[28] J. P. Abriata and J. C. Bolcich, The Nb-Zr (Niobium-Zirconium) System. Bulletin of Alloy Phase Diagrams 3 (1982) 34-44

[29] E. Francis, R. Prasath Babu, A. Harte, T.L. Martin, P. Frankel, D. Jädernäs, J. Romero, L. Hallstadius, P.A.J. Bagot, M.P. Moody, M. Preuss, Effect of Nb and Fe on damage evolution in a Zr-alloy during proton and neutron irradiation, Acta Mater. 165 (2019) 603-614

[30] Y. Matsukawa, H.L. Yang, K. Saito, Y. Murakami, T. Maruyama, T. Iwai, K. Murakami, Y. Shinohara, T. Kido, T. Toyama, Z. Zhao, Y.F. Li, S. Kano, Y. Satoh, Y. Nagai, H. Abe, The effect of crystallographic mismatch on the obstacle strength of second phase precipitate particles in dispersion strengthening: bcc Nb particles and nanometric Nb clusters embedded in hcp Zr, Acta Mater. 102 (2016) 323-332

[31] E.A. Marquis, J.M. Hyde, Applications of atom-probe tomography to the characterisation of solute behaviours, Mater. Sci. Eng. R 69 (2010) 37–62

[32] S. Lozano-Perez, 13: Characterization techniques for assessing irradiated and ageing materials in nuclear power plant systems, structures and components (SSC), in: Philip G. Tipping (Ed.), Understanding and Mitigating Ageing in Nuclear Power Plants, Woodhead Publishing Limited, UK, 2010, pp. 389-416

[33] G. Cliff, G. W. Lorimer, The quantitative analysis of thin specimens, J. Microsc. 103 (1975) 203-207

[34] D.B. Williams, C.B. Carter, Transmission Electron Microscopy: A Textbook for Materials Science, 1996, Springer, New York.

[35] D.E. Newbury, N.W.M. Ritchie, Performing elemental microanalysis with high accuracy and high precision by scanning electron microscopy/silicon drift detector energy-dispersive X-ray spectrometry (SEM/SDD-EDS), J. Mater. Sci. 50 (2015) 493-518

[36] N.W.M. Ritchie, Spectrum Simulation in DTSA-II, Microsc. Microanal. 15 (2009) 454-468

[37] J. Végh, I. Kadar, S. Ricz, B. Sulik, D. Varga, G. Székely, A reliability test of measured spectra, Nucl. Instr. Meth. A 281 (1989) 605-609

---

[38] E. Smith, J. Nutting, Direct carbon replicas from metal surfaces, British J. Appl. Phys. 7 (1956) 214-217

[39] G. Neumann, C. Tuijn, Self-diffusion and impurity diffusion in pure metals: Handbook of experimental data, first ed., Pergamon, Oxford, 2009.

[40] S. Banerjee, R. Krishnan, Martensitic transformation in Zirconium-Niobium alloys, Acta Met. 19 (1971) 1317-1326

[41] S. Banerjee, S.J. Vijayakar, R. Krishnan, Precipitation in zirconium-niobium martensites, J. Nucl. Mater. 62 (1976) 229-239

[42] H.G. Kim, Y.H. Jeong, T.H. Kim, Effect of isothermal annealing on the corrosion behavior of Zr–xNb alloys, J. Nucl. Mater. 326 (2004) 125-131

[43] A. Harte, M. Griffiths, M. Preuss, The characterization of second phases in the Zr-Nb and Zr-Nb-Sn-Fe alloys: A critical review, J. Nucl. Mater. 505 (2018) 227-239

[44] O.T. Woo, M. Griffiths, The role of Fe on the solubility of Nb in α-Zr, J. Nucl. Mater. 384 (2009) 77-80

[45] M.S. Granovsky, M. Canay, E. Lena, D. Arias, Experimental investigation of the Zr corner of the ternary Zr-Nb-Fe phase diagram, J. Nucl. Mater. 302 (2002) 1-8.

[46] C. Ramos, C. Saragovi, M.S. Granovsky, Some new experimental results on the Zr-Nb-Fe system, J. Nucl. Mater. 366 (2007) 198-205

[47] P. Barberis, D. Charquet, V. Rebeyrolle, Ternary Zr-Nb-Fe(O) system: phase diagram at 853 K and corrosion behaviour in the domain Nb < 0.8%, J. Nucl. Mater. 326 (2004) 163-174

[48] C. Toffolon-Masclet, T. Guilbert, J.C. Brachet, Study of secondary intermetallic phase precipitation/dissolution in Zr alloys by high temperature-high sensitivity calorimetry, J. Nucl. Mater. 372 (2008) 367-378

Highlights

- EDS/TEM experimental Cliff-Lorimer factors for Zr-Nb-Ta alloys
- Equilibrium microstructure at 570 °C in (α+β) Zr-Nb-Ta alloys
- Change of Nb solute concentration in the α-Zr matrix by adding Ta to Zr-1Nb alloy
- Change of Zr concentration in β-Nb precipitates by adding Ta to Zr-1Nb alloy
- Zirconium apex of the ternary Zr-Nb-Ta system

Declaration of interests

☒ The authors declare that they have no known competing financial interests or personal relationships that could have appeared to influence the work reported in this paper.

☐The authors declare the following financial interests/personal relationships which may be considered as potential competing interests:

Declarations of interest: none